

Evolution of electronic and ionic structure of Mg -clusters with the growth cluster size

Andrey Lyalin,^{*} Ilia A Solov'yov,[†] Andrey V Solov'yov,[‡] and Walter Greiner

Institut für Theoretische Physik der Universität Frankfurt am Main,

Robert-Mayer Str. 8-10, D-60054 Frankfurt am Main, Germany

The optimized structure and electronic properties of neutral and singly charged magnesium clusters have been investigated using *ab initio* theoretical methods based on density-functional theory and systematic post-Hartree-Fock many-body perturbation theory accounting for *all* electrons in the system. We have systematically calculated the optimized geometries of neutral and singly charged magnesium clusters consisting of up to 21 atoms, electronic shell closures, binding energies per atom, ionization potentials and the gap between the highest occupied and the lowest unoccupied molecular orbitals. We have investigated the transition to the *hcp* structure and metallic evolution of the magnesium clusters, as well as the stability of linear chains and rings of magnesium atoms. The results obtained are compared with the available experimental data and the results of other theoretical works.

I. INTRODUCTION

Metal clusters have been recognized as new physical objects with their own properties almost two decades ago. This became clear after such experimental successes as the discovery of electronic shell structure in metal clusters [1], observation of plasmon resonances [2, 3, 4], formation of singly and doubly charged negative cluster ions [5] and many more.

^{*}Permanent address: Institute of Physics, St Petersburg State University, 198504 St Petersburg, Petrodvorez, Russia; Email address: lyalin@th.physik.uni-frankfurt.de

[†]Permanent address: A. F. Ioffe Physical-Technical Institute, 194021 St. Petersburg, Russia; Email address: ilia@th.physik.uni-frankfurt.de

[‡]Permanent address: A. F. Ioffe Physical-Technical Institute, 194021 St. Petersburg, Russia; Email address: solovyov@th.physik.uni-frankfurt.de

Comprehensive survey of the field can be found in review papers and books; see, e.g., [6, 7, 8, 9, 10, 11, 12, 13, 14].

The electronic shell structure of metal clusters has been discovered in [1] by the observation of the strong peaks in the mass spectra of sodium clusters. The enhanced stability of some clusters, the so-called magic clusters, was explained by the closure of shells of delocalized electrons. A simple physical model describing electronic shell structure of metal clusters has been developed within the jellium approximation (see, e.g., [6]) by analogy with the shell model of atomic nuclei (see, e.g., [15]). The jellium model is very successful for the simple alkali metals (Na , K), for which one electron per atom is delocalized [16, 17, 18]. The jellium model electronic shell closures for alkali-metal clusters define the magic numbers $N = 8, 20, 34, 40, 58, 92$ that are in a good agreement with experiment. Note that the jellium model can be generalized by accounting for the collective ion background vibration dynamics [19, 20] and be used as a very appropriate framework for the investigating collision processes involving atomic clusters [21].

Clusters of divalent metals are expected to differ from the jellium model predictions at least at small cluster sizes. In this case, bonding between atoms is expected to have some features of the van der Waals type of bonding, because the electronic shells in the divalent atoms are filled. Thus, clusters of divalent metals are very appropriate for studying non-metal to metal transition, testing different theoretical methodologies and conceptual developments of atomic cluster physics. However, relatively little work was done so far on the exploration of the alkali-earth metal clusters in comparison with that for the alkali-metal clusters; see, e.g., [6, 22] and references therein.

Previous theoretical studies of the magnesium cluster properties have been performed using pseudopotential approximation for the treatment of inner electrons in a cluster and the density-functional theory for the description of outer shell electrons. The electronic properties, geometry and stability of small Mg metal clusters with the number of atoms $N \leq 7$ have been investigated in [23, 24] using the pseudopotential local-spin-density approximation. The geometrical structure and bonding nature of Mg_N clusters with N up to 13 have been studied in [25] using the density-functional molecular-dynamics method. The size evolution of bonding in magnesium clusters Mg_N with $N = 8 - 13, 16, 20$ have been studied in [26] using the local-density approximation that accounts for gradient corrections. Structural and electronic properties of small magnesium clusters ($N \leq 13$) were studied in

[27] using a first-principles simulation method in conjunction with the density-functional theory and the generalized gradient correction approximation for the exchange-correlation functional. It was shown [27] that the metallization in magnesium clusters has a slow and nonmonotonic evolution, although, also jellium-type magic clusters were observed [25, 26]. In order to extend such calculations to larger systems, symmetry restricted methods have been developed. The spherically-averaged-pseudo-potential scheme with the local and non-local pseudopotentials has been used for the investigation of the electronic structure and shell closures of spherical Mg_N clusters up to $N = 46$ [28].

Recently, new experimental data for Mg clusters have been obtained, indicating the most intensive pics in the mass spectra at $N = 5, 10, 15, 18, 20, 25, 28, 30, 35, 40, 47, 56, 59, 62,$ and 69 [29]. These numbers deviate from the sequence of magic numbers which were obtained for simple alkali metal clusters, and cannot be reproduced within simple jellium models. This fact was interpreted in [29, 30] within the spherical shell model by diving of the high angular momentum states down through the states with lower l .

In the present work we investigate the optimized ionic structure and the electronic properties of neutral and singly charged magnesium clusters within the size range $N \leq 21$. We calculate binding energies per atom, ionization potentials and energy gaps between the highest occupied and the lowest unoccupied molecular orbitals. Our calculations are based on *ab initio* theoretical methods invoking the density-functional theory and systematic post-Hartree-Fock many-body theory accounting for *all* electrons in the system. The results obtained are compared with the available experimental data and the results of other theoretical works.

The atomic system of units, $|e| = m_e = \hbar = 1$, has been used throughout the paper, unless other units are indicated.

II. THEORETICAL METHODS

Our calculations have been performed with the use of the Gaussian 98 software package [31]. We have utilized the $6 - 311G(d)$ basis set of primitive Gaussian functions to expand the cluster orbitals [31, 32].

The cluster geometries have been determined by finding local minima on the multidimensional potential energy surface for a cluster. We have taken into account *all electrons*

available in the system, when computing the potential energy surface. With increasing cluster size, such calculations become computer time demanding. In this work, we limit the calculations by the cluster size $N = 21$.

The key point of calculations is fixing the starting geometry of the cluster, which could converge during the calculation to a local or the global minimum. There is no unique way for achieving this goal with *Gaussian 98* [32]. In our calculations, we have created the starting geometries empirically, often assuming certain cluster symmetries. Note, that during the optimization process the geometry of the cluster as well as its initial symmetry sometimes change dramatically. All the characteristics of clusters, which we have calculated and present in next section, are obtained for the clusters with optimized geometry.

In this work we concentrate on the systematic exploration of the properties of magnesium clusters using the density-functional theory based on the hybrid Becke-type three-parameter exchange functional [33] paired with the gradient-corrected Lee, Yang and Parr correlation functional (*B3LYP*) [34, 35], as well as the gradient-corrected Perdew-Wang 91 correlation functional (*B3PW91*) [36, 37]. The important feature of the density-functional method consists in the fact that it takes into account many-electron correlations via the phenomenological exchange-correlation potential. However, so far, there has not been found the unique potential, universally applicable for different systems and conditions. As a result there are many different parameterizations for the exchange-correlation potential valid for special cases.

Alternatively, we use a direct *ab initio* method for the description of electronic properties of metal clusters, which is based on the consistent post-Hartree-Fock many-body theory [38]. In the present work, we apply the Møller-Plesset perturbation theory of the fourth order (*MP4*). Based on the fundamental physical principles being free from any phenomenological parameters, this model can be refined by extending the quality of the approximations, while the physical meaning of the effects included is clearly demonstrated. Thus, often such an approach predicts more accurate and reliable characteristics of metal clusters than the density-functional theory.

In the present work we use both different theoretical schemes for calculations taking advantage of the clear physical meaning and reliability of the post-Hartree-Fock perturbation theory and the numerical efficiency of the density-functional methods.

III. NUMERICAL RESULTS AND DISCUSSION

A. Geometry optimization of Mg_N and Mg_N^+ clusters

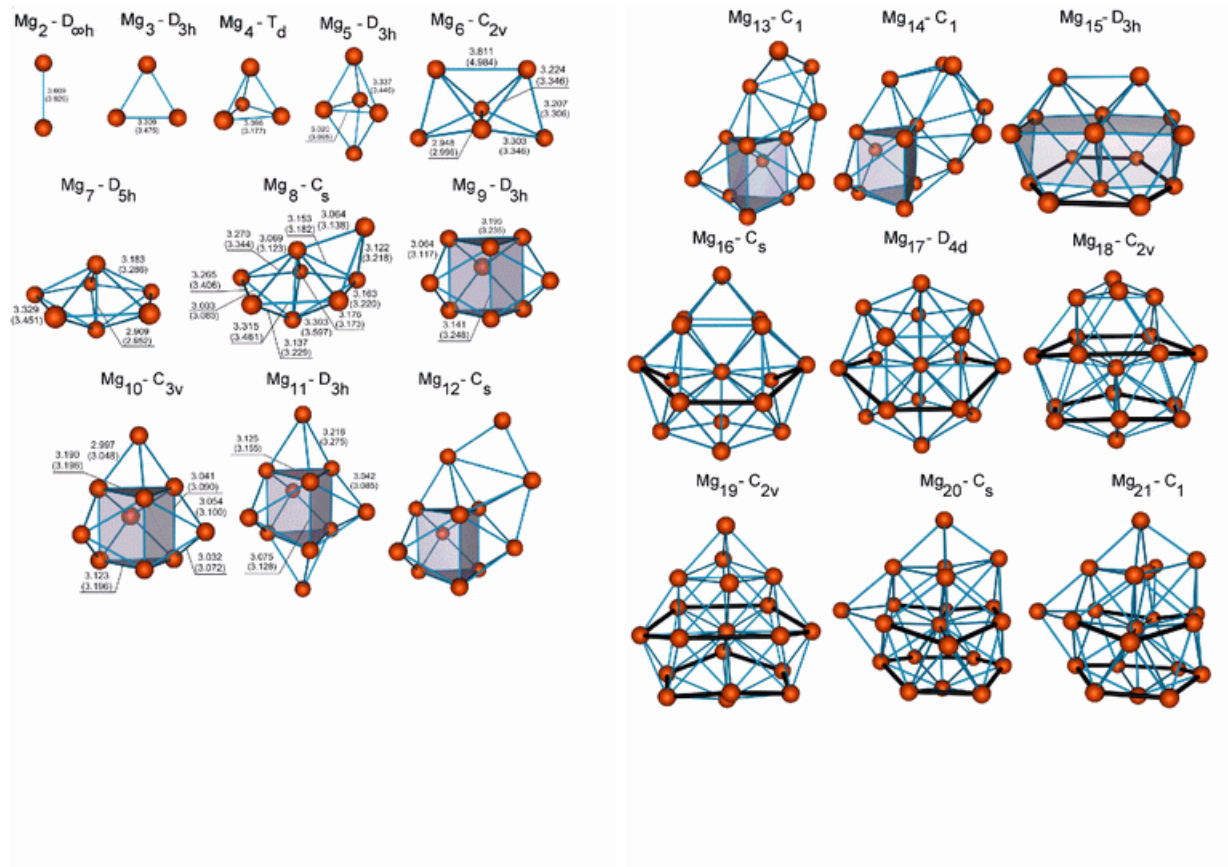


FIG. 1: Optimized geometries of the neutral magnesium clusters $Mg_2 - Mg_{21}$ calculated in the $B3PW91$ approximation. The interatomic distances are given in angstroms. The values in brackets correspond to the $B3LYP$ results. The label above each cluster image indicates the point symmetry group of the cluster.

The optimization of the cluster geometries has been performed with the use of the $B3PW91$ and $B3LYP$ methods. For small magnesium clusters with number of atoms $N \leq 11$, we have also used the *ab initio* $MP4$ method in addition to density-functional calculations. With the growth cluster size the *ab initio* $MP4$ calculations become more and more computer time demanding, therefore we have not performed such calculations for magnesium clusters with the number of atoms $N \geq 12$. The detail comparison of the results obtained by the density-functional and *ab initio* perturbation theory methods as well

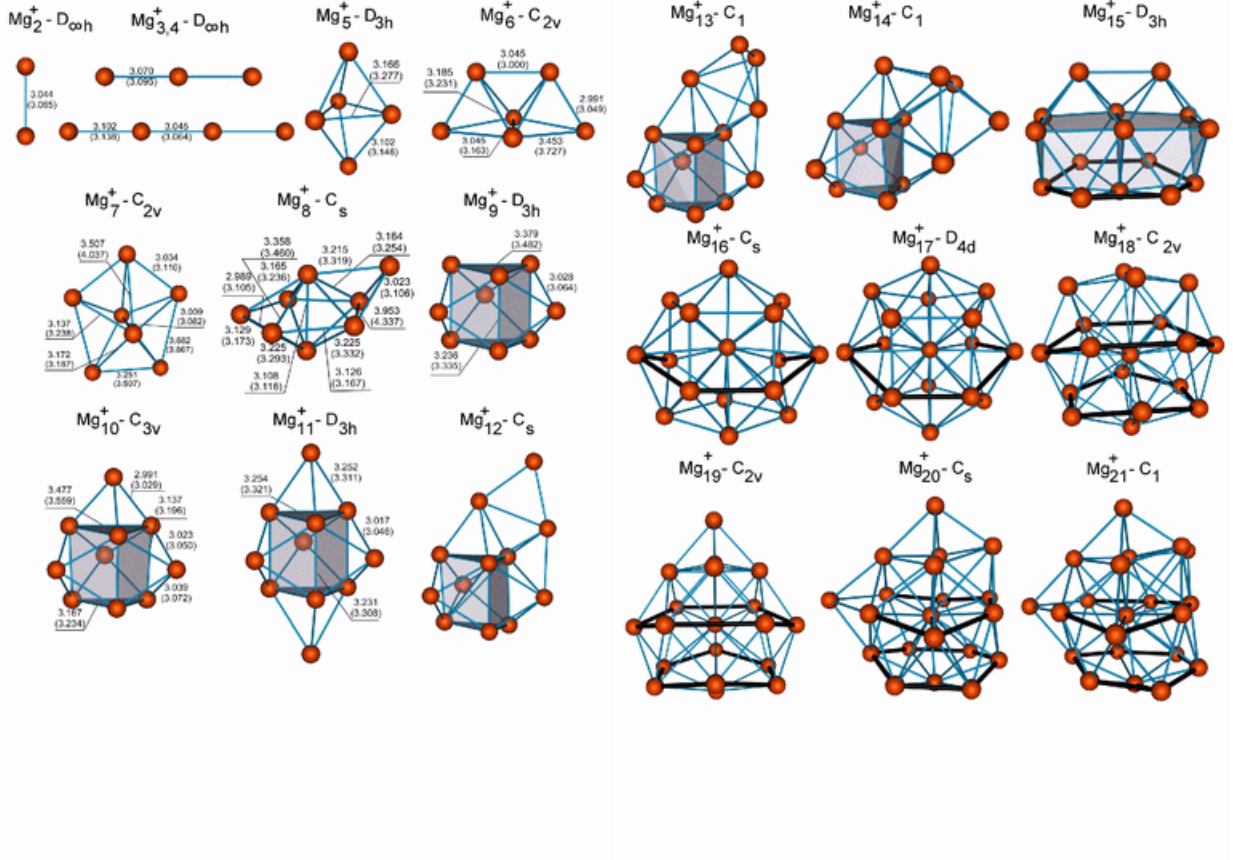


FIG. 2: The same as in Fig.1 but for singly-charged magnesium clusters $Mg_2^+ - Mg_{21}^+$.

as their comparison with the results of other works is given below, see section III B. This comparison allows us to conclude that for magnesium clusters the *B3PW91* method is more reliable and accurate in comparison with the *B3LYP* one.

The results of the cluster geometry optimization for neutral and singly charged magnesium clusters consisting of up to 21 atoms are shown in figures 1 and 2 respectively.

Magnesium clusters possess various isomer forms those number grows dramatically with increasing cluster size. In figures 1 and 2, we present only the lowest energy configurations optimized by the *B3PW91* method. The interatomic distances are given in angstroms. The values in brackets correspond to the interatomic distances obtained by the *B3LYP* method.

Figure 1 shows that the neutral magnesium clusters form the compact structures, maximizing the coordination number. The Mg_2 dimer is weakly bound possessing the binding energy per atom 0.039 eV/atom and the bond length 3.609 Å, which is in a good agreement with the experimental results of Ref. [39], where the values 0.025 eV/atom for the binding

energy and 3.89 Å and for the bond length have been reported. The lowest energy state for Mg_3 is the equilateral triangle, and for Mg_4 is a regular tetrahedron. As we discuss below, the Mg_4 cluster is relatively more stable and compact, as compared to the neighbouring clusters. The Mg_5 cluster has a structure of slightly elongated triangular bipyramid, while Mg_6 consists of three pyramids connected by their faces, Mg_7 is a pentagonal bipyramid, and Mg_8 is a capped pentagonal bipyramid. These geometrical structures are in a good agreement with the results of Ref. [25].

It is worth to note that the optimized geometry structures for small neutral magnesium clusters differ significantly from those obtained for sodium clusters (see, e.g., [22, 40, 41] and references therein). Thus, the optimized sodium clusters with $N \leq 6$ have the plane structure. For Na_6 , both plane and spatial isomers with very close total energies exist. The planar behavior of small sodium clusters has been explained as a result of the successive filling of the 1σ and 1π symmetry orbitals by delocalized valence electrons [40], which is fully consistent with the deformed jellium model calculations [18]. Contrary to the small sodium clusters, the magnesium clusters are tri-dimensional already at $N = 4$, forming the structures nearly the same as the van der Waals bonded clusters.

Starting from Mg_9 a new element appears in the magnesium cluster structures. This is the six atom trigonal prism core, which is marked out in figure 1. The formation of the trigonal prism plays the important role in the magnesium cluster growth process. Adding an atom to one of the triangular faces of the trigonal prism of the Mg_9 cluster results in the Mg_{10} structure, while adding an atom to the remaining triangular face of the prism within the Mg_{10} cluster leads to the structure of Mg_{11} , as shown in figure 1.

Further growth of the magnesium clusters for $12 \leq N \leq 14$ leads to the formation of the low symmetry ground state cluster. In spite of their low symmetry, all these clusters have the trigonal prism core. The structural rearrangement occurs for the Mg_{15} cluster, which results in the high symmetry structure of the two connected Mg_9 clusters.

Starting from Mg_{15} another motif based on the hexagonal ring structure which is marked out in figure 1 dominates the cluster growth. Such a ring is the basic element of the hexagonal closest-packing (*hcp*) lattice, as one can see in figure 3, in which the primitive cell for the magnesium *hcp* lattice is presented. Thus, $N = 15$ is the turning-point in the formation of the *hcp* lattice for magnesium.

Vectors **a**, **b** and **c** in figure 3 show the primitive cell axes of the *hcp* lattice. For bulk

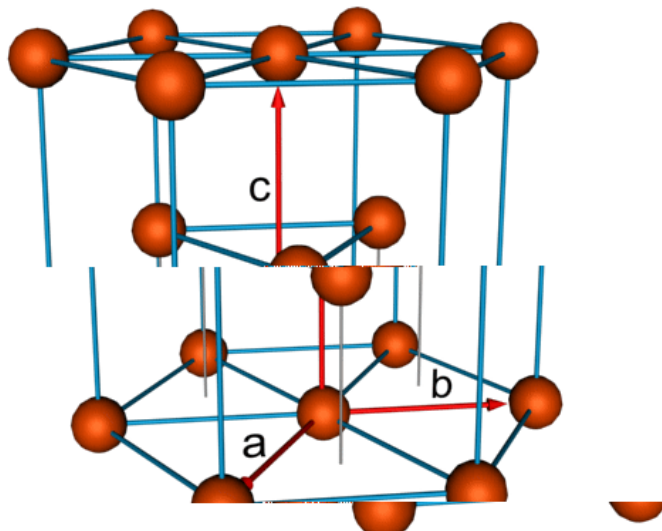


FIG. 3: Primitive cell for magnesium *hcp* lattice. For bulk magnesium $a = b = 3.21 \text{ \AA}$ and $c = 5.21 \text{ \AA}$ [42].

magnesium $a = b = 3.21 \text{ \AA}$ and $c = 5.21 \text{ \AA}$ [42]. The fundamental characteristic for the hexagonal closest-packing of spheres is the value of ratio c/a , which is equal to $\sqrt{8/3} \approx 1.633$ for ideal *hcp* lattice. The bulk magnesium with $c/a = 1.62$ is very close to ideal *hcp* structure [43].

The distinct three-layered structure of Mg -clusters with $N \geq 18$ based on the hexagonal rings allows one to determine the averaged values of the primitive axes $\langle c \rangle$ and $\langle a \rangle$. Table I demonstrates that the calculated values $\langle c \rangle$ and $\langle a \rangle$ and their ratio for magnesium clusters with $N \geq 18$ are very close to the corresponding values for bulk magnesium.

Figure 2 shows the optimized geometries of singly-charged cationic magnesium clusters. The ground state geometries of the cationic magnesium clusters are not very different from those obtained for the neutral parent clusters with the exception of Mg_3^+ and Mg_4^+ , the equilibrium geometries of which are linear chains. Below, we discuss the stability of the linear chain isomers for the magnesium clusters (neutral and singly-charged) within the size range considered.

In figure 4, we present the average bonding distance, $\langle d \rangle$, calculated within the *B3PW91*

TABLE I: The averaged values of the primitive axes and its ratio for the *hcp* lattice element for magnesium clusters with $N \geq 18$ calculated within the *B3PW91* approximation. Values in brackets correspond to singly-charged magnesium clusters.

	Mg_{18}	Mg_{19}	Mg_{20}	Mg_{21}	Mg bulk, [42]
$\langle c \rangle$, Å	5.08 (5.42)	5.47 (5.37)	5.48 (5.23)	5.56 (5.23)	5.21
$\langle a \rangle$, Å	3.14 (3.19)	3.05 (3.22)	3.20 (3.21)	3.20 (3.21)	3.21
$\langle c \rangle / \langle a \rangle$	1.62 (1.70)	1.79 (1.67)	1.71 (1.63)	1.74 (1.63)	1.62

approximation for neutral and singly-charged magnesium clusters. When calculating the average bonding distance in a cluster, interatomic distances smaller than 4.1 Å have only been taken into account. The bulk limit for the magnesium *hcp* lattice [42] indicated in figure by horizontal dashed line.

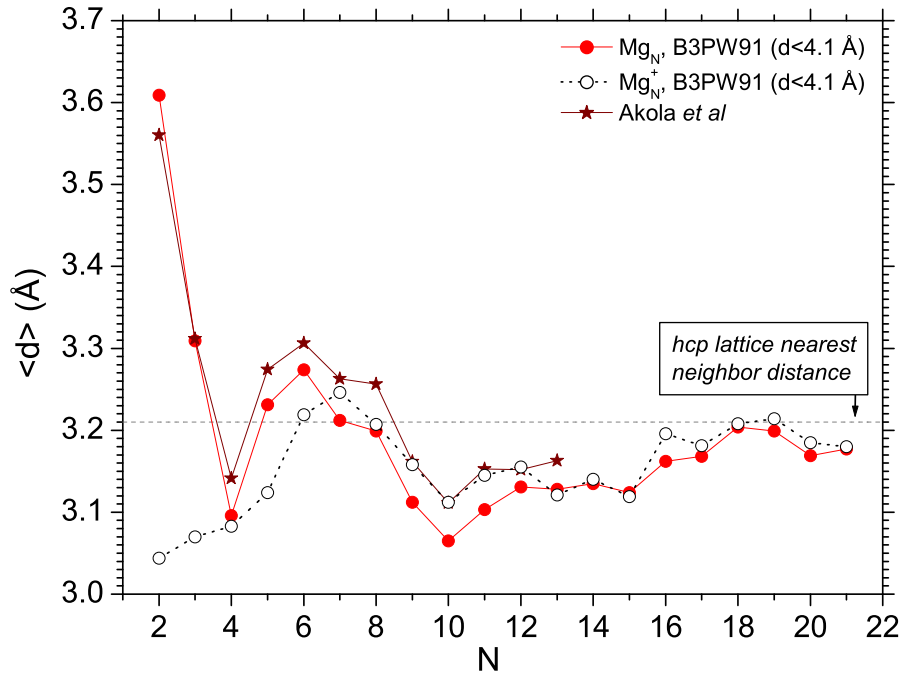


FIG. 4: The average bonding distance as a function of cluster size for neutral and singly-charged magnesium clusters. Stars present the results of the work by Akola *et al* [27]. The horizontal dashed line indicates the bulk limit for the *hcp* lattice [42].

Figure 4 shows how the average bonding distance evolve with increasing cluster size. It is clearly seen that the dependence of the average bonding distance on cluster size has essentially non-monotonous oscillatory behavior. For Mg_2 , the bonding distance calculated within the *B3PW91* method is equal to 3.609 Å, which is in a good agreement with the experimental result 3.891 Å of Ref. [39]. The appearance of the minima in the size dependence of the average bonding distance shows that Mg_4 , Mg_{10} , and Mg_{20} clusters (8, 20 and 40 valence electrons, respectively) are more tightly packed than their neighbours. This behavior can be interpreted by the influence of electronic shell effects on the geometrical structure of magnesium clusters. It supports the conclusion of Ref. [44] that electronic shell effects can enhance the stability of geometric structures resulting from dense ionic packing.

Additional minimum in the dependence of the average bonding distance on N arises at $N = 15$. At this N a considerable rearrangement of the cluster geometry take place as it is seen from figure 1. Indeed, starting from the Mg_{15} cluster the three-layered structure based on the hexagonal ring is formed. It is clearly seen in figure 4 that for $N \geq 15$ the average bonding distance for magnesium clusters approaches the bulk limit.

The evolution of the average bonding distance with cluster size differs for magnesium clusters from that for sodium. For neutral sodium clusters, one can see odd-even oscillations of $\langle d \rangle$ atop its systematic growth and approaching the bulk limit [22]. These features have the quantum origin and arise due to the spin coupling of the delocalized valence electrons. For magnesium clusters, the average bonding distance depends on size non-monotonically, with minima for the Mg_4 , Mg_{10} , Mg_{15} , and Mg_{20} clusters. Such an irregular behavior is induced by both the closure of electronic shells of the delocalized electrons and structural rearrangements.

Manifestation of the magic numbers in the dependence of the average bonding distance on cluster size coinciding with the spherical jellium model magic numbers does not imply, however, the rapid metallization of magnesium clusters. To investigate the transition of van der Waals to metal bonding in magnesium clusters it is necessary to explore in detail the evolution of their electronic properties. Below we perform such analysis in detail.

Dashed line in figure 4 shows the average bonding distance as a function of cluster size calculated for singly-charged magnesium clusters. Figure 4 demonstrates the essential difference in the cluster size dependence of $\langle d \rangle$ for the cationic and neutral magnesium clusters with $N \leq 6$. The small cationic magnesium clusters are more compact in comparison with

the corresponding neutral clusters. For example, for Mg_2^+ the bonding distance is equal to 3.044 Å, which is much less than in the case of Mg_2 . This phenomenon has a simple physical explanation: the removed electron is taken from the antibonding orbital. The fact that cationic magnesium clusters are more stable than the parent neutral and anionic clusters has been already noted in [24].

Within the size range $N \geq 7$, the average bonding distances for single-charged and neutral magnesium clusters behave similarly. The absolute value of $\langle d \rangle$ for single-charged clusters is slightly larger in this region of N .

Figure 4 demonstrates the good agreement of our results with the dependence of $\langle d \rangle$ on N calculated in [27] for neutral Mg -clusters within the size range $N \leq 13$.

B. Binding energy per atom for Mg_N and Mg_N^+ clusters.

The binding energy per atom for small neutral and singly-charged magnesium clusters is defined as follows:

$$E_b/N = E_1 - E_N/N \quad (1)$$

$$E_b^+/N = ((N - 1)E_1 + E_1^+ - E_N^+)/N, \quad (2)$$

where E_N and E_N^+ are the energies of a neutral and singly-charged N -particle atomic cluster, respectively. E_1 and E_1^+ are the energies of a single magnesium atom and an ion.

Figures 5 and 6 show the dependence of the binding energy per atom for neutral and singly-charged clusters as a function of cluster size. The energies of clusters have been obtained using the *B3LYP*, *B3PW91* and *MP4* methods. Calculations of the binding energies have been performed by different theoretical methods and with the use of different exchange-correlation functionals for the sake of comparison of their accuracy and computation efficiency. In figure 5 filled rhombus, crossed rhombus and opened pentagons show the result of calculations by Kumar *et al* [25], Reuse *et al* [24] and Delaly *et al* [26] respectively. These calculations have been performed within the Hohenberg-Kohn-Sham local-density approximation using the Perdew and Zunger [45] parameterization of the Ceperley and Alder [46] data for the exchange correlations. Crossed circles and stars present the results of Delaly *et al* [26] and Akola *et al* [27] derived with the use of the gradient-corrected approximation [47, 48] and the PBE parameterization of the gradient-corrected exchange-correlation energy

functional [49] respectively.

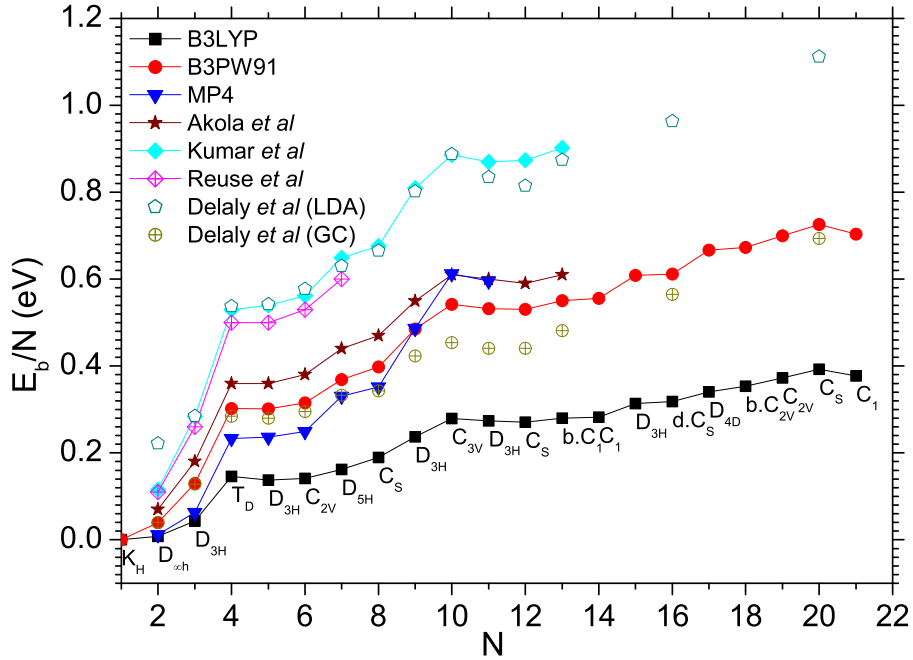


FIG. 5: Binding energy per atom for neutral magnesium clusters as a function of cluster size. Squares, circles and lower triangles represent the binding energies per atom calculated by the *B3LYP*, *B3PW91* and *MP4* methods respectively. Stars, filled rhombus and crossed rhombus show the results of the works by Akola *et al* [27], Kumar *et al* [25], and Reuse *et al* [24] respectively. Opened pentagons and crossed circles show the result of Delaly *et al* [26] obtained with the use of the LDA and gradient-corrected (GC) LDA methods respectively. Labels indicate the point symmetry group of the isomers represented. Their geometries one can find in section III A.

Figure 5 shows that, although, the qualitative behavior of the binding energy per atom calculated within different approaches is similar, the quantitative discrepancy between the curves is rather considerable. This is a result of different accounting for the gradient corrections to the local-density exchange correlation interaction within different methods. The gradient corrections have been shown to provide a systematic improvement in the computed properties of magnesium clusters [26]. The difference in the binding energy per atom for neutral magnesium clusters with $N \leq 21$ calculated with the use of the gradient corrected *B3LYP* and *B3PW91* methods reaches 0.35 eV. The reason for this difference is in the

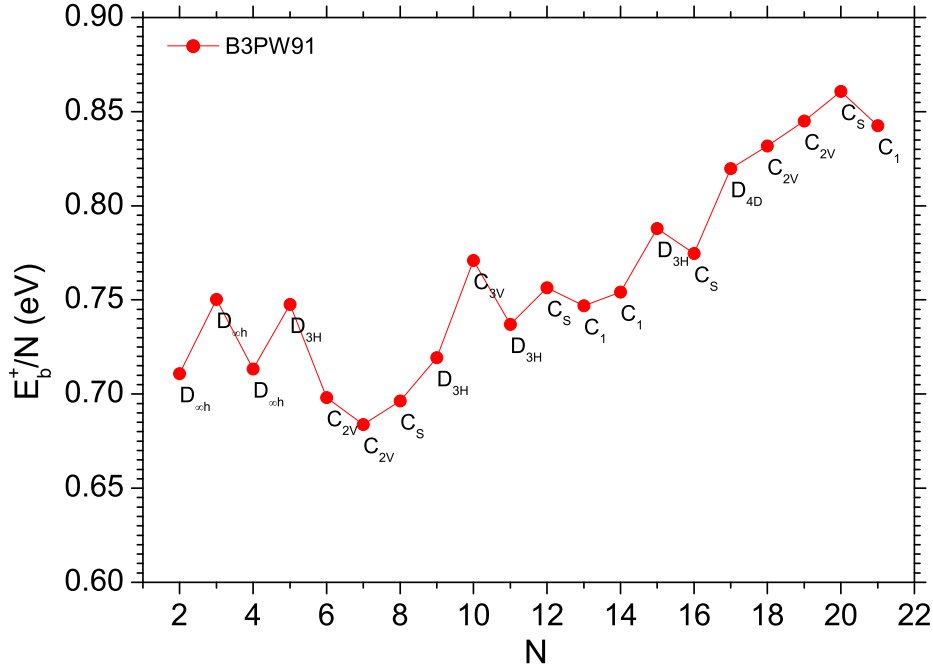


FIG. 6: The same as in Fig.5 but for singly-charged magnesium clusters.

different way of accounting for many-electron correlations within the *B3LYP* and *B3PW91* methods. To explore what type of parameterization of the exchange-correlation energy is more reliable for magnesium clusters we have used the post-Hartree-Fock Møller-Plesset perturbation theory. This method is free of phenomenological parameters and can be used as a criterion for checking the reliability of various density-functional theory schemes. The disadvantage of the perturbation theory approach consists in the fact that it leads to the dramatic growth of the computational costs with increasing the number of electrons in the system in comparison with that for the density-functional theory calculations. Therefore, we have used the *MP4* method only for clusters with the number of atoms $N \leq 11$.

Figure 5 shows that the results of the *MP4* theory are in a reasonable agreement with those derived by the *B3PW91* method. This comparison demonstrates that for magnesium clusters simulations the *B3PW91* method is more reliable than the *B3LYP* one. Our results derived within the *B3PW91* and *MP4* approximations are in a good agreement with those from Ref. [26, 27].

We now discuss the behavior of the binding energy as a function of cluster size for both

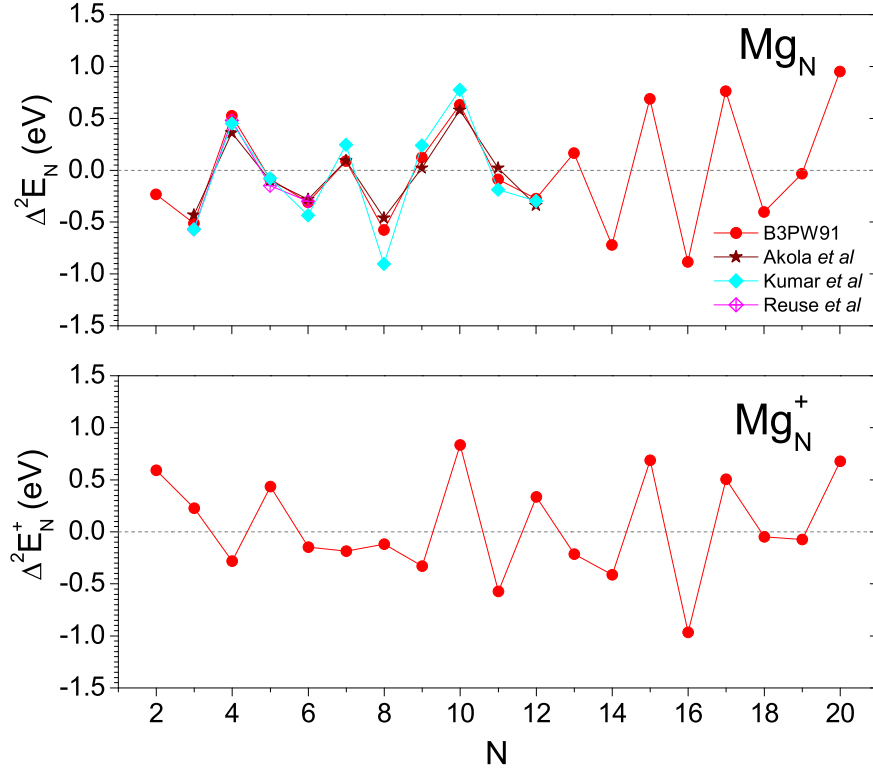


FIG. 7: Second differences of total energy for neutral, $\Delta^2 E_N = E_{N+1} - 2E_N + E_{N-1}$, and singly-charged, $\Delta^2 E_N^+ = E_{N+1}^+ - 2E_N^+ + E_{N-1}^+$, magnesium clusters. Stars show the result of the work by Akola *et al* [27], filled rhombus by Kumar *et al* [25], and crossed rhombus by Reuse *et al* [24].

neutral and singly-charged magnesium clusters. For neutral magnesium clusters, the binding energy per atom increases steadily with the growth cluster size. The local maxima of E_b/N at $N = 4, 10$ and 20 correspond to the most stable configurations of the magic magnesium clusters possessing $N_{el} = 8, 20$ and 40 valence electrons respectively. This behavior is in agreement with the simple spherical jellium model. The analysis of the second differences of the binding energy (see Fig.7) confirms this conclusion and makes a hint about relative stability of the Mg_7, Mg_{13}, Mg_{15} , and Mg_{17} clusters, in addition to the magic clusters Mg_4, Mg_{10} and Mg_{20} . The additional magic numbers can be explained within the deformed jellium model accounting for spheroidal deformations of the cluster core (see, e.g., [16, 17, 18] and references therein). For a spheroidal jellium cluster, the orbital angular momentum does not remain a good quantum number characterizing the valence electrons energy levels. In

this case, the energy levels are characterized by the projection of the angular momentum Λ on the principal axis and by the parity of the wave function. Thus, the energy levels with $\Lambda = 0$ are twofold degenerated on the projection of the electron's spin, while those with $\Lambda \neq 0$ are fourfold degenerated both on the projection of the electron spin and on the sign of the projection Λ on the principal cluster axis. The deformed jellium clusters having closed electronic subshells possess the enhanced stability. Therefore, in addition to the spherical magic clusters with 8, 20, 40 etc valence electrons, the deformed jellium clusters with 6, 10, 14, 18, 22, 26, 30, 34 etc. valence electrons turn out to be relatively stable. This fact leads to the following additional magic numbers 3, 5, 7, 9, 11, 13, 15, 17 for the jellium magnesium clusters. Some of these numbers, such as 3, 5, 9, 11 precede or follow the spherical magic numbers 4, 10, 20 and as a result of that become masked and are not that pronounced in the second differences analysis.

For singly-charged magnesium clusters, the binding energy per atom as a function of cluster size is essentially non-monotonous. The local maxima of the binding energy for the Mg_3^+ , Mg_5^+ , Mg_{10}^+ , Mg_{12}^+ , Mg_{15}^+ and Mg_{20}^+ clusters indicate their enhanced stability. Figure 7 shows second differences of the total energy for singly-charged magnesium clusters. This figure demonstrates the enhanced stability of the mentioned cluster ions and the Mg_{17}^+ cluster.

The sequence of magic numbers for singly charged magnesium clusters differs from that for neutral clusters. This happens because singly charged magnesium clusters always possess odd number of valence electrons and, thus, always contain open electronic shells. For neutral magnesium clusters, situations of both close and open electronic shells are possible. The enhanced stability of a Mg -cluster ion arises, when its electronic configuration has one hole in or an extra electron above the filled shells. Thus, the cluster ions Mg_5^+ , Mg_{11}^+ and Mg_{21}^+ contain one extra electron over the completed spherical electronic shells, while the clusters Mg_4^+ , Mg_{10}^+ and Mg_{20}^+ have a hole in the spherical outer electronic shell. Our results presented in figures 6 and 7 demonstrate that the cluster ions Mg_5^+ , Mg_{10}^+ and Mg_{20}^+ turn out to be more stable than their neighbors. We note that the alteration of the magic number from $N = 4$ for neutral Mg -clusters to $N = 5$ for Mg -cluster ions happens because the electronic configuration containing an extra electron becomes more favorable for Mg_5^+ . This is not the case for the Mg_{10}^+ and Mg_{20}^+ clusters, those outer electronic configurations contain a hole.

The Mg -cluster mass spectra have been recorded in [29] indicating the enhanced stability of the clusters with $N = 5, 10, 15, 18$ and 20 . In that work the role of the cluster ionization was not reliably clarified [29] and thus the charge state of the clusters was not reliably determined. As a result, the observed magic numbers sequence should be a combination of the magic numbers sequences for neutral and singly-charged cluster ions. Thus, $N = 5$ is the ionic magic number, $N = 10, 15$ and 20 are the magic numbers manifesting themselves clearly for both neutral Mg -clusters and Mg -cluster ions. The second differences are positive and relatively large for $N = 13$ (neutral clusters) and $N = 12$ (singly-charged cluster ions). Possibly, the interplay between neutral clusters and ions make these numbers masked in experiment. The second differences are also positive for $N = 7$ for neutral Mg -clusters and for $N = 3$ for Mg -cluster ions, although the enhancement for those numbers have not been experimentally observed. We explain this fact by possible suppression of the experimental signal in the region of small N and relatively small values of the second differences in the mentioned cases.

The potential energy surface for a cluster becomes more and more complicated with increasing cluster size. The magnesium clusters are not an exception. Figure 8 demonstrates this fact where we present the binding energies per atom calculated for a variety of isomers of neutral magnesium clusters. The corresponding point symmetry groups and the accurate values of the total energies calculated within the $B3LYP$ and $B3PW91$ approximations are presented in Appendix in tables II and III respectively. Most of the isomer configurations have been obtained using the $B3LYP$ method, while the $B3PW91$ method has been used for the exploration of the ground state energy isomers, as well as for the linear and ring-like isomer structures.

Squares in figure 8 correspond to the most stable clusters possessing the minimal total energy. Among the variety of isomers, presented in figure 8, we mark certain groups of isomers with the fixed symmetry. So, circles present the linear chains ($D_{\infty h}$ point symmetry group) and the upper triangles correspond to the rings of N atoms (D_{Nh} point symmetry group). It is an interesting fact that among the multitude of the isomers of neutral magnesium clusters the linear chains and rings are always stable. We pay a particular attention to these structures because of their possible applications in nano-technology. Extracting these isomers and putting them on a substrate one can produce one-atom wide quantum wires. The linear chains and rings of atoms are also very interesting from the theoretic-

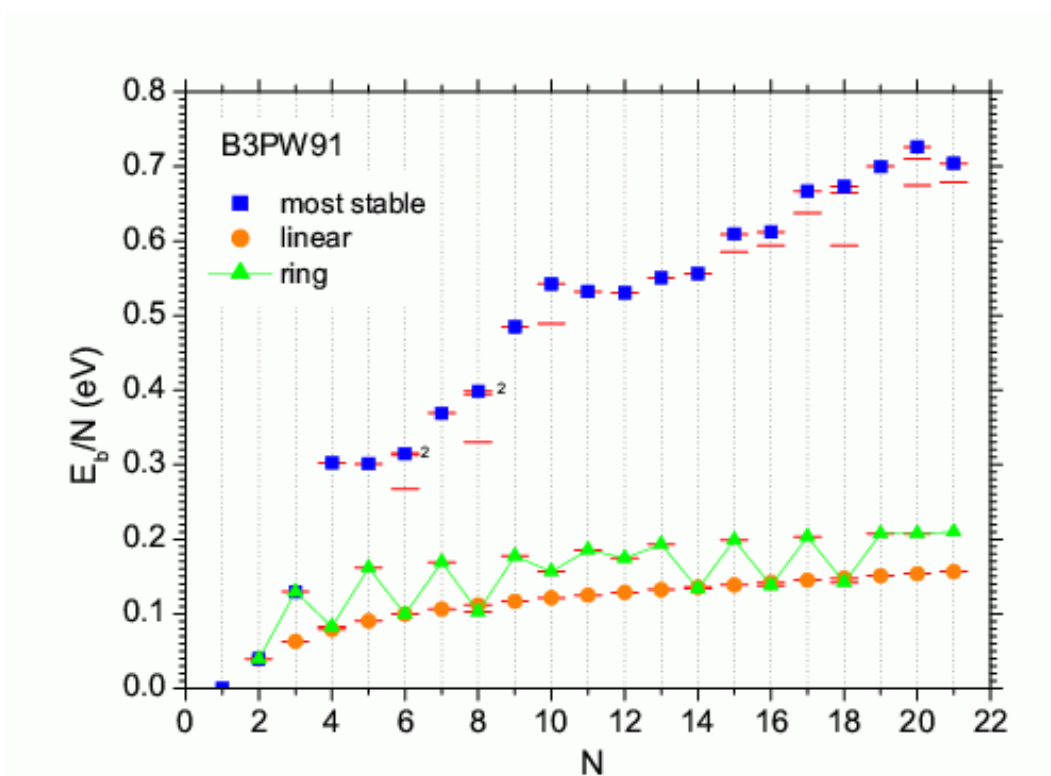
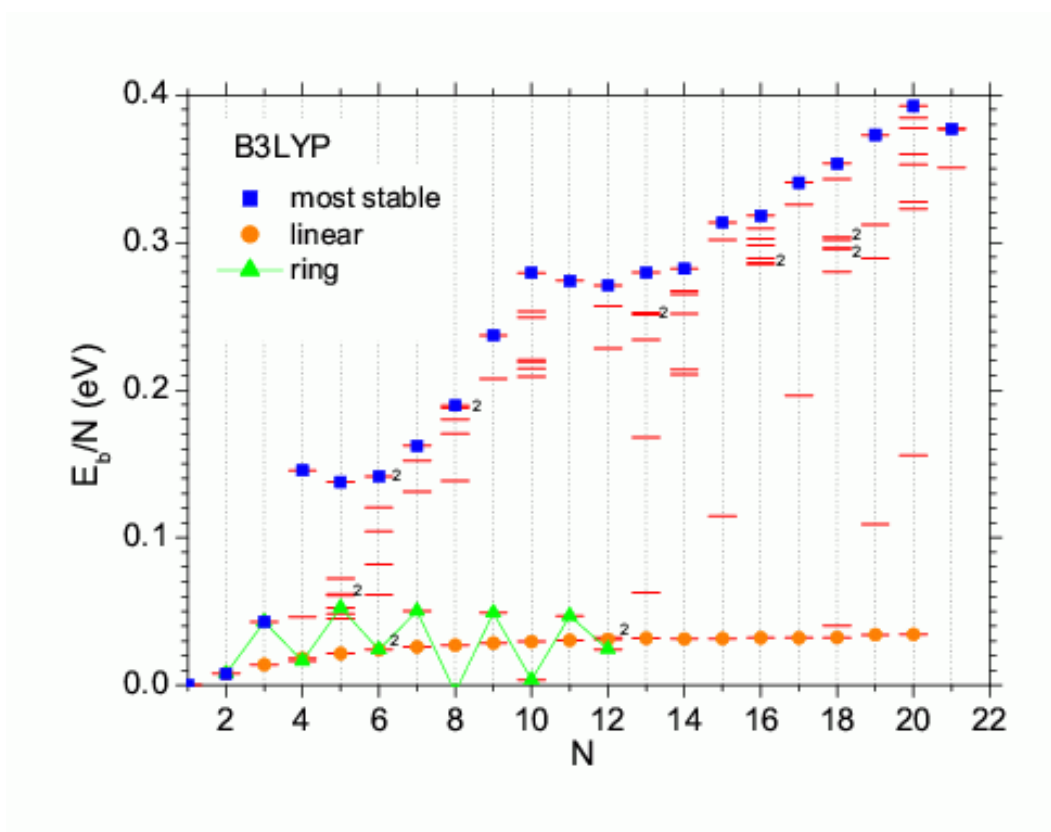


FIG. 8: Binding energy per atom for a variety of isomers of neutral magnesium clusters as a function of cluster size. The corresponding point symmetry groups and the accurate values of the total energies are presented in Appendix in tables II and III. Numbers near some lines show the number of found isomers with the corresponding close energies.

cal point of view, because with their help one can investigate the transition from one- to two-dimensional structures. For linear chains, the binding energy per atom increases slowly with the growth the number of atoms, while in the case of rings the value of E_b/N has the prominent odd-even oscillatory behavior.

This behavior arises as a result of successive filling the σ - and π -symmetry orbitals by valence electrons in magnesium linear chains and rings. Indeed, because of its symmetry the one-dimensional linear chain of N magnesium atoms has the following configuration of valence electrons: $1\sigma^2, 2\sigma^2, 3\sigma^2, \dots, N\sigma^2$. Therefore for any N it has the closed electronic shell structure. This fact explains the monotonous growth with N of the linear chain binding energy, and its relative saturation in the region $N > 10$.

The molecular orbitals for the structure of the ring-type have to be aligned with the plane of the ring. Such orbitals are fourfold degenerated due to symmetry reasons. The Mg_2 dimer has four valence electrons that occupy spherically-shaped $1\sigma^2$ and prolate-like $2\sigma^2$ orbitals. The Mg_3 trimer has six valence electrons, two of them occupy $1\sigma^2$ state, while the remaining four electrons fill the fourfold degenerated $1\pi^4$ orbital aligned with the plane of the trimer. With increasing the number of magnesium atoms in the ring, the valence electrons continue to occupy fourfold degenerated orbitals aligned with the plane of the ring. Therefore, in the magnesium ring-like isomers with the odd number of atoms all electronic shells are closed, while the isomers with the even number of atoms have the open electronic shell. This fact results in the enhanced stability of the magnesium rings with an odd number of atoms $N = 3, 5, 7, 9, \dots$ etc. and explains the odd-even oscillatory behavior of the binding energy for the magnesium rings.

C. Ionization potentials and HOMO-LUMO gaps

Let us now consider how the ionization potential of magnesium clusters evolves with increasing cluster size. The ionization potential of a cluster V_i is equal to the difference between the energies of the corresponding cluster ion and the neutral cluster, $V_i = E_N^+ - E_N$. Figure 9 shows the dependence of the adiabatic V_i^{adiab} (i.e. the geometry relaxation of the ionized cluster is taken into account) and vertical V_i^{vert} (i.e. the cluster geometry is frozen during the ionization process) ionization potential on N . We compare our results derived by the *B3PW91* method with theoretical data from Ref. [27] and [24] and with the bulk

limit, $V_i^{bulk} = 3.64$ eV, taken from [42].

Both the vertical and adiabatic ionization potentials evolve non-monotonously with increasing cluster size. Figure 9 shows that ionization potential of magnesium clusters steadily but rather slow decreases towards the bulk limit. This evolution is neither rapid nor monotonous process. In order to exclude the influence of the cluster geometry rearrangement, we first consider the vertical ionization potential. The size dependence of the vertical ionization potential has a prominent maximum at $N = 4$ followed by a sharp decrease. Such a behavior of the ionization potential is typical for the jellium model, predicting maxima in the size dependence of the ionization potential at the magic numbers corresponding to the clusters with closed electronic shells. Our data are in a good agreement with the results of Ref. [24], but contradict to those reported in Ref. [27] for the Mg_3 and Mg_4 clusters. In [27] the appearance of the deep minimum in vertical ionization potential at $N = 4$ was explained as a result of a stronger charge delocalization in the Mg_4 cluster in comparison with its neighbours.

We note that the peculiarities in the ionization potential dependence on N correlate with the magic numbers that appear for the singly-charged magnesium clusters. Indeed, the minima in V_i^{vert} correspond to the maxima in E_b^+/N for Mg -cluster ions (see Fig. 6). This fact has a simple explanation. The ionization potential of a cluster is equal to the difference between the energies of the corresponding cluster ion and the neutral cluster. For neutral Mg -clusters, the binding energy as a function of N increases steadily with the growth cluster size, while for Mg -cluster ions - irregularly. Thus, their difference mimics all the irregularities that appear in the binding energy dependence on N for singly-charged magnesium clusters.

For $N \geq 6$, the vertical ionization potential changes slowly with increasing cluster size. This process is characterized by the irregularities that originate due to the influence of the cluster geometry on the jellium-type electronic structure of Mg -clusters.

Indeed, the shape of a jellium cluster is defined by its electronic structure. Thus, the closed shell jellium clusters are spherical, while clusters with opened electronic shells are deformed due to the Jahn-Teller distortions. The jellium picture works fairly well for sodium clusters. The ionization potential of sodium clusters drops rapidly and systematically at the electronic shell closures. The N -dependence of the ionization potential has prominent, regular odd-even oscillations (see, e.g., [18, 22] and references therein). Magnesium clusters are

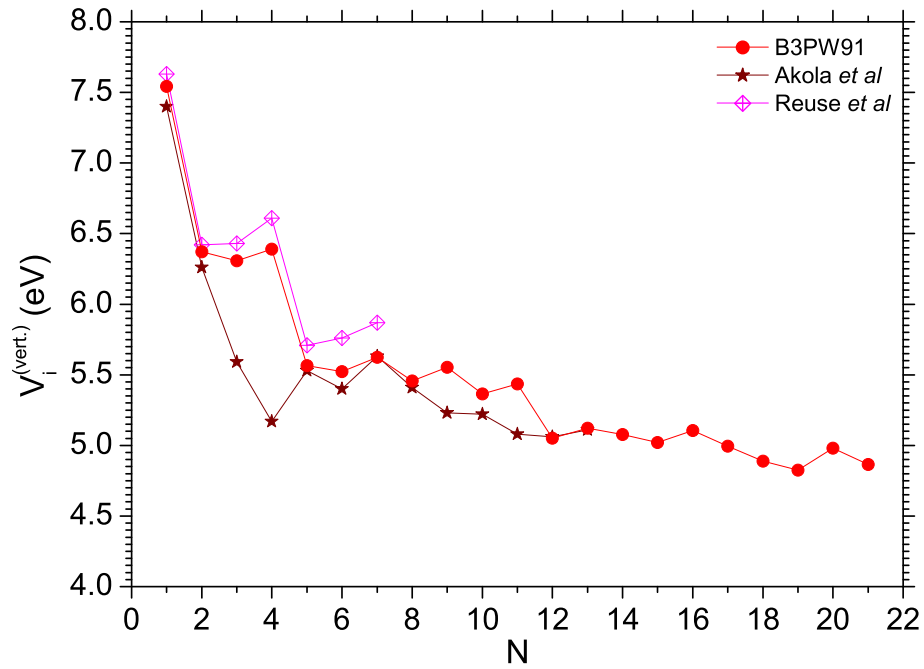
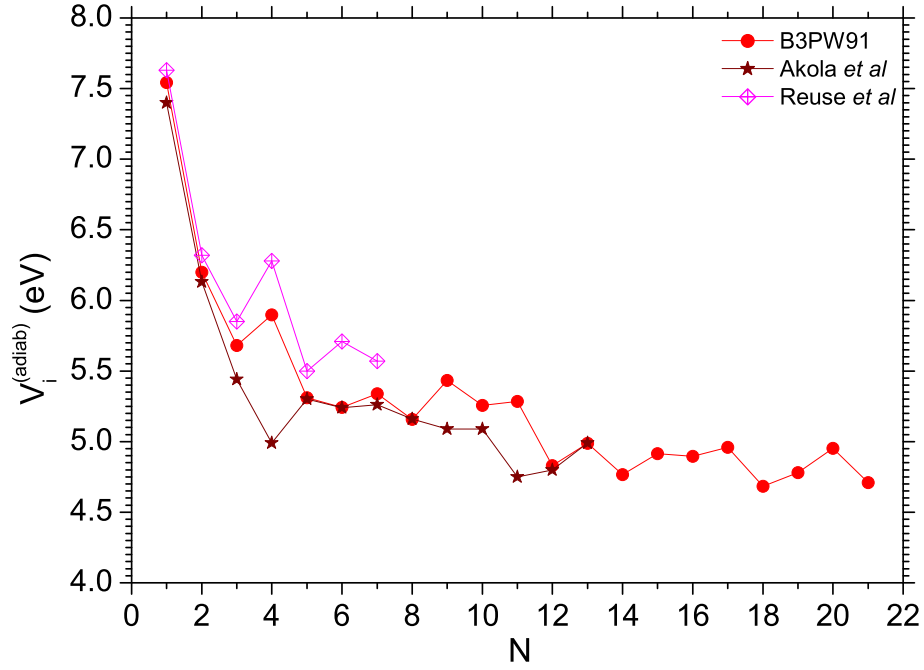


FIG. 9: Adiabatic, V_i^{adiab} , and vertical, V_i^{vert} , ionization potential for small magnesium clusters. Stars and crossed rhombus show the result of the work by Akola *et al* [27] and by Reuse *et al* [24] respectively.

different. As discussed in section III A, the evolution of the Mg -cluster geometry is closely connected with the formation of elements of the hcp lattice cell. Although, the electronic shell effects clearly manifest themselves in the formation of the Mg -cluster geometry, they do not determine it completely. Another words, there is an interplay of the jellium and the hcp lattice factors in the formation of the Mg -cluster geometry and the electronic properties such as the binding energy and the ionization potential.

The adiabatic ionization potential dependence that is shown in figure 9 exhibits qualitatively the same behavior as the vertical one, however, has more pronounced irregularities due to geometry rearrangements of the ionized clusters.

Figure 10 shows the gap E_g between the highest occupied and the lowest unoccupied molecular orbitals (HOMO-LUMO gap) for the Mg -clusters as a function of cluster size. For the sake of comparison, we have also calculated the HOMO-LUMO gap for the sodium clusters and present it in figure 10. Calculations have been performed using the $B3PW91$ and $B3PLYP$ methods. The geometries of neutral sodium clusters have been taken from [22]. For the small magnesium clusters with $N \leq 13$, we compare our results with those presented in Ref. [27].

The size dependence of E_g for neutral sodium clusters has an oscillatory behavior with local maxima at $N = 6, 8, 10, 14$ and 20 . These maxima correspond to the electronic shell closures in a full accordance with the deformed jellium model. The local maximum in the size dependence of E_g at $N = 12$ and the shift of the local maximum from $N = 18$ to $N = 17$ are the consequences of triaxial deformations [22]. Thus, the triaxial deformation leads to the splitting of the fourfold degenerated highest occupied orbital on two twofold degenerated orbitals. As a result of that the additional shell closure at the $N_{el} = 12$ appears.

For Mg -clusters, the evolution of the HOMO-LUMO gap with the growth cluster size differs from that for Na -clusters. The gap E_g calculated for magnesium clusters shows the oscillatory behavior accompanied by the gradual decrease in the absolute value. Maxima in this dependence at $N = 4, 10$ and 20 correspond to the magic numbers of the spherical jellium model ($N_{el} = 8, 20$ and 40 respectively). The similar feature also does exist for Na -clusters at $N = 8$ and 20 . Additional variation of E_g appears both due the subshell closures and the cluster structural rearrangements.

We note that the HOMO-LUMO gap remains rather large even for the clusters with $N \geq 15$ possessing elements of the hcp lattice of the bulk Mg . This fact confirms the

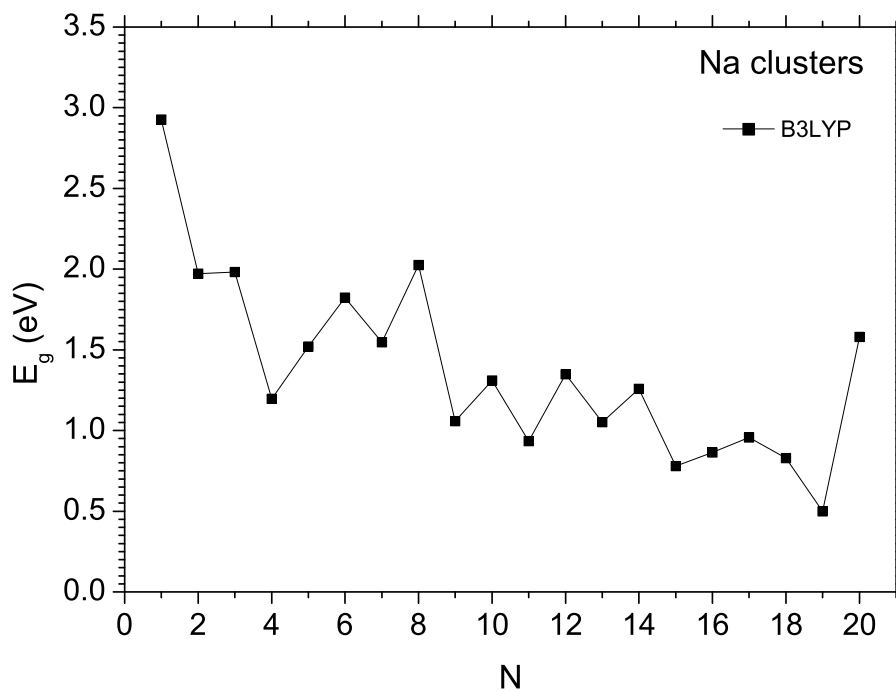
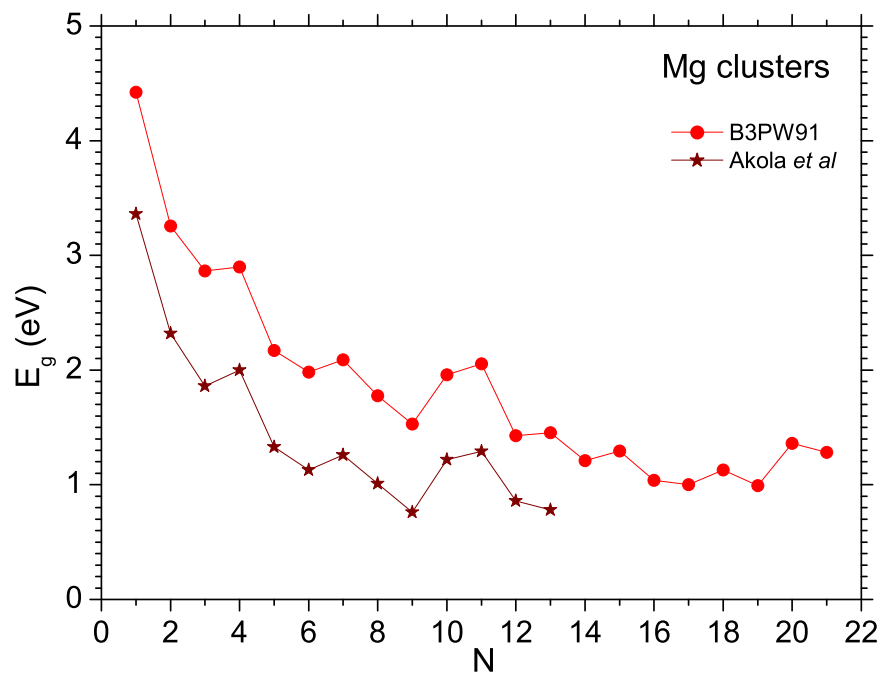


FIG. 10: Gap between the highest occupied and the lowest unoccupied eigenstates for the Mg and Na clusters as a function of cluster size. Circles and squares represent the HOMO-LUMO gap calculated by the $B3PW91$ and the $B3LYP$ methods respectively. Stars show the result of the work by Akola *et al* [27].

conclusion on the slow and non-monotonous evolution of metallic properties in Mg clusters.

IV. CONCLUSION

The optimized geometries and electronic properties of neutral and singly-charged magnesium clusters consisting of up to 21 atoms have been investigated using the $B3PW91$, $B3LYP$ and $MP4$ methods accounting for all electron in the system. The detailed comparison of the results of the phenomenological $B3PW91$ and $B3LYP$ density-functional methods with the results of the systematic *ab initio* post-Hartree-Fock many-body theory leads us to the conclusion that the $B3PW91$ method is more reliable for Mg -cluster simulations than the $B3LYP$ one.

We have investigated the size evolution of the Mg -clusters geometry. It has been shown that starting from Mg_{15} the hexagonal ring structure determines the cluster growth, which is the basic element of the *hcp* lattice for the bulk magnesium.

We have investigated the electronic properties of magnesium clusters. It has been shown that the electronic shell effects and jellium-like behavior clearly manifest themselves in the formation of geometrical properties, however, the shell effects do not determine the geometry of Mg clusters completely. We have demonstrated that due to the interplay of the jellium and the *hcp* lattice factors the electronic properties of magnesium clusters possess irregularities which can not be explained within the simple jellium model. It has been shown that the metallic evolution of magnesium clusters is slow and non-monotonous process.

The results of this work can be extended in various directions. One can use the similar methods to study structure and properties of various types of clusters. It is interesting to extend calculations towards larger cluster sizes and to perform more advanced comparison of model and *ab initio* approaches. A lot of novel problems arise, when considering collisions and electron excitations in the clusters with the optimized geometries [21]. These and many more other problems on atomic cluster physics can be tackled with the use of methods considered in our work.

Acknowledgments

The authors acknowledge support from the Alexander von Humboldt Foundation and the Russian Academy of Sciences (Grant 44).

APPENDIX

TABLE II: Total energies and the point symmetry groups for a variety of isomers of neutral magnesium clusters. Calculations have been done by the *B3LYP* method.

N	Point group	Energy (a.u.)	N	Point group	Energy (a.u.)	N	Point group	Energy (a.u.)
1		-200.0931	9	$D_{\infty h}$	-1800.8472	16	$d.C_s$	-3201.6766
2	$D_{\infty h}$	-400.1868	10	C_{3v}	-2001.0336		$c.C_s$	-3201.6713
3	D_{3h}	-600.2840		C_{4v}	-2001.0239		$b.C_1$	-3201.6673
	$D_{\infty h}$	-600.2807		T_d	-2001.0225		$a.C_1$	-3201.6646
4	T_d	-800.3938		C_1	-2001.0120		T_d	-3201.6594
	D_{2h}	-800.3792		D_{3h}	-2001.0114		$a.C_s$	-3201.6579
	$D_{\infty h}$	-800.3750		C_{2v}	-2001.0098		$b.C_s$	-3201.6572
	D_{4h}	-800.3748		D_{4d}	-2001.0078		$D_{\infty h}$	-3201.5082
5	D_{3h}	-1000.4907		$D_{\infty h}$	-2000.9417	17	D_{4d}	-3401.7953
	C_{4v}	-1000.4787		D_{10h}	-2000.9322		C_s	-3401.7861
	T_d	-1000.4768	11	D_{3h}	-2201.1348		D_{3h}	-3401.7052
	C_{2v}	-1000.4766		D_{11h}	-2201.0430		$D_{\infty h}$	-3401.6026
	D_{5h}	-1000.4751		$D_{\infty h}$	-2201.0362	18	$b.C_{2v}$	-3601.9095
	D_{2D}	-1000.4743	12	$a.C_s$	-2401.2366		$c.C_s$	-3601.9026
	D_{2h}	-1000.4738		$b.C_s$	-2401.2304		C_2	-3601.8764
	$D_{\infty h}$	-1000.4694		C_{2v}	-2401.2178		$b.C_s$	-3601.8752
6	C_{2v}	-1200.5898		D_{6h}	-2401.1313		$a.C_s$	-3601.8716
	D_{2h}	-1200.5897		$D_{\infty h}$	-2401.1308		$a.C_{2v}$	-3601.8711
	D_{4h}	-1200.5851		D_{12h}	-2401.1278		D_{5h}	-3601.8608
	C_{5v}	-1200.5815	13	$b.C_1$	-2601.3438		D_{6h}	-3601.7022
	D_{3h}	-1200.5765		C_S	-2601.3308		$D_{\infty h}$	-3601.6970
	O_h	-1200.5720		$a.C_1$	-2601.3302	19	C_{2v}	-3802.0292
	D_{6h}	-1200.5639		C_{3v}	-2601.3221		C_{3v}	-3801.9867
	$D_{\infty h}$	-1200.5638		I_h	-2601.2904		D_{5h}	-3801.9706
7	D_{5h}	-1400.6933		D_{6h}	-2601.2401		D_{6h}	-3801.8449
	C_3	-1400.6908		$D_{\infty h}$	-2601.2253		$D_{\infty h}$	-3801.7925
	C_{3v}	-1400.6854	14	C_1	-2801.4485	20	C_s	-4002.1503
	D_{7h}	-1400.6645		$b.C_{3v}$	-2801.4397		C_1	-4002.1444
	$D_{\infty h}$	-1400.6583		C_s	-2801.4407		$d.C_{2v}$	-4002.1392
8	$a.C_{2v}$	-1600.7999		C_{2v}	-2801.4328		$c.C_{2v}$	-4002.1263
	C_s	-1600.7976		O_h	-2801.4115		$b.C_{2v}$	-4002.1212
	$b.C_{2v}$	-1600.7948		$a.C_{3v}$	-2801.4134		T_d	-4002.1026
	T_d	-1600.7854		$D_{\infty h}$	-2801.3194		$a.C_{2v}$	-4002.0990
	$D_{\infty h}$	-1600.7527	15	D_{3h}	-3001.5692		D_{6h}	-4001.9764
9	D_{3h}	-1800.9162		C_s	-3001.5627		$D_{\infty h}$	-4001.8870
	C_{3v}	-1800.9064		D_{6h}	-3001.4594	21	C_1	-4202.2460
	D_{9h}	-1800.8540		$D_{\infty h}$	-3001.4138		C_{2v}	-4202.2255

TABLE III: The same as table II but for the *P3PW91* method.

N	Point group	Energy (a.u.)	N	Point group	Energy (a.u.)
1		-200.0379	14	C_1	-2800.8170
2	$D_{\infty h}$	-400.0788		$D_{\infty h}$	-2800.6007
3	D_{3h}	-600.1281		D_{14h}	-2800.5997
	$D_{\infty h}$	-600.1207	15	D_{3h}	-3000.9045
4	T_d	-800.1962		C_s	-3000.8914
	D_{4h}	-800.1638		D_{15h}	-3000.6786
	$D_{\infty h}$	-800.1633		$D_{\infty h}$	-3000.6453
5	D_{3h}	-1000.2450	16	$d.C_s$	-3200.9666
	D_{5h}	-1000.2193		$c.C_s$	-3200.9560
	$D_{\infty h}$	-1000.2063		$D_{\infty h}$	-3200.6902
6	C_{2v}	-1200.2970		D_{16h}	-3200.6880
	D_{2h}	-1200.2966	17	D_{4d}	-3401.0612
	C_{5v}	-1200.2865		C_s	-3401.0428
	D_{6h}	-1200.2495		D_{17h}	-3400.7719
	$D_{\infty h}$	-1200.2495		$D_{\infty h}$	-3400.7353
7	D_{5h}	-1400.3604	18	$b.C_{2v}$	-3601.1279
	D_{7h}	-1400.3091		$c.C_s$	-3601.1221
	$D_{\infty h}$	-1400.2928		$b.C_s$	-3601.0756
8	C_s	-1600.4205		$D_{\infty h}$	-3600.7806
	$a.C_{2v}$	-1600.4193		D_{18h}	-3600.7766
	T_d	-1600.4005	19	C_{2v}	-3801.2093
	$D_{\infty h}$	-1600.3364		D_{19h}	-3800.8653
	D_{8h}	-1600.3335		$D_{\infty h}$	-3800.8260
9	D_{3h}	-1800.5018	20	C_s	-4001.2920
	D_{9h}	-1800.4000		C_1	-4001.2801
	$D_{\infty h}$	-1800.3800		$b.C_{2v}$	-4001.2539
10	C_{3v}	-2000.5786		D_{20h}	-4000.9111
	T_d	-2000.5590		$D_{\infty h}$	-4000.8716
	D_{10h}	-2000.4367	21	C_1	-4201.3398
	$D_{\infty h}$	-2000.4238		C_{2v}	-4201.3201
11	D_{3h}	-2200.6322			
	D_{11h}	-2200.4923			
	$D_{\infty h}$	-2200.4678			
12	$a.C_s$	-2400.6891			
	D_{12h}	-2400.5321			
	$D_{\infty h}$	-2400.5119			
13	$b.C_1$	-2600.7561			
	D_{13h}	-2600.5853			
	$D_{\infty h}$	-2600.5562			

References

- [1] W.D. Knight, K. Clemenger, W.A. de Heer, W.A. Saunders, M.Y. Chou and M.L. Cohen, *Phys. Rev. Lett.* **52**, 2141 (1984).
- [2] C. Bréchnignac, Ph. Cahuzac, F. Carlier, J. Leygnier, *Chem. Phys. Lett.* **164**, 433 (1989).
- [3] K. Selby, M. Vollmer, J. Masui, V. Kresin, W.A. de Heer and W.D. Knight, *Phys. Rev. B* **40**, 5417 (1989).
- [4] K. Selby, V. Kresin, J. Masui, M. Vollmer, W.A. de Heer, A. Scheidemann, W.D. Knight, *Phys. Rev. B* **43**, 4565 (1991).
- [5] A. Herlert, S. Krückeberg, L. Schweikhard, M. Vogel, C. Walther, *Physica Scripta T* **80**, 200 (1999)
- [6] W. Ekardt (ed.), *Metal Clusters* (Wiley, New York, 1999).
- [7] *Atomic Clusters and Nanoparticles*, NATO Advanced Study Institute, les Houches Session LXXIII, les Houches, 2000, edited by C. Guet, P. Hobza, F. Spiegelman and F. David (EDP Sciences and Springer Verlag, Berlin, 2001).
- [8] W.A. de Heer, *Rev. Mod. Phys.* **65**, 611 (1993).
- [9] M. Brack, *Rev. Mod. Phys.* **65**, 677 (1993).
- [10] C. Bréchnignac, J.P. Connerade, *J.Phys.B:At.Mol.Opt.Phys.* **27**, 3795 (1994).
- [11] H. Haberland (ed.), *Clusters of Atoms and Molecules, Theory, Experiment and Clusters of Atoms*, (Springer Series in Chemical Physics, Berlin **52**, 1994).
- [12] U. Näher, S. Bjørnholm, S. Frauendorf, F. Garcias and C. Guet, *Physics Reports* **285**, 245 (1997).
- [13] J. Jellinek (ed.), *Theory of Atomic and Molecular Clusters. With a Glimpse at Experiments*, (Springer Series in Cluster Physics, Berlin, 1999).
- [14] K-H. Meiwes-Broer (ed.), *Metal Clusters at Surfaces. Structure, Quantum Properties, Physical Chemistry*, (Springer Series in Cluster Physics, Berlin, 1999).
- [15] J.M. Eisenberg, and W. Greiner, *Nuclear Theory. Vol.1. Collective and Particle Models*, (North Holland, Amsterdam, 1985).
- [16] A.G. Lyalin, S.K. Semenov, A.V. Solov'yov, N.A. Cherepkov and W. Greiner, *J. Phys. B* **33**,

- 3653 (2000).
- [17] A.G. Lyalin, S.K. Semenov, A.V. Solov'yov, N.A. Cherepkov, J.-P. Connerade, and W. Greiner, *J. Chin. Chem. Soc. (Taipei)* **48**, 419 (2001).
- [18] A. Matveentsev, A. Lyalin, I.A. Solov'yov, A.V. Solov'yov and W. Greiner, submitted to *Int. Journal of Modern Physics E* (2002); LANL preprint arXiv:physics/0207085 v2, 26 July 2002 (<http://arxiv.org>).
- [19] L.G. Gerchikov, A.V. Solov'yov, W. Greiner, *International Journal of Modern Physics E* **8**, 289 (1999).
- [20] L.G. Gerchikov, A.N. Ipatov, A.V. Solov'yov and W. Greiner, *J. Phys. B: At. Mol. Opt. Phys.* **33**, 4905 (2000).
- [21] A.V. Solov'yov, in *Atomic Clusters and Nanoparticles* (Ref.[7]).
- [22] I.A. Solov'yov, A.V. Solov'yov and W. Greiner, *Phys. Rev. A* **65**, 053203 (2002).
- [23] F. Reuse, S.N. Khanna, V. de Coulon and J. Buttet *Phys. Rev. B* **39**, 12911 (1989).
- [24] F. Reuse, S.N. Khanna, V. de Coulon and J. Buttet *Phys. Rev. B* **41**, 11743 (1990).
- [25] V. Kumar and R. Car *Phys. Rev. B* **44**, 8243 (1991).
- [26] P. Delaly, P. Ballone and J. Buttet *Phys. Rev. B* **45**, 3838 (1992).
- [27] J. Akola, K.Rytkönen and M. Manninen *Eur. Phys. J. D* **16**, 21 (2001).
- [28] Li. Serra, P.-G. Reinhard and E. Suraud *Eur. Phys. J. D* **18**, 327 (2002).
- [29] Th. Diederich, T. Döppner, J. Braune, J. Tiggesbäumker and K.-H. Meiwes-Broer, *Phys. Rev. Lett.* **86**, 4807 (2001).
- [30] T. Döppner, T. Diederich, J. Tiggesbäumker and K.-H. Meiwes-Broer, *Eur. Phys. J. D* **16**, 13 (2001).
- [31] M.J. Frisch *et al*, computer code GAUSSIAN 98, Rev. A. 9, Gaussian Inc., Pittsburgh, PA, 1998.
- [32] James B. Foresman and Æleen Frisch *Exploring Chemistry with Electronic Structure Methods* (Pittsburgh, PA: Gaussian Inc, 1996)
- [33] A.D. Becke, *Phys.Rev. A* **38**, 3098 (1988).
- [34] C. Lee, W. Yang and R.G. Parr, *Phys. Rev. B* **37**, 785 (1988).
- [35] R.G. Parr and W. Yang, *Density-Functional Theory of Atoms and Molecules*, (Oxford University Press, Oxford, New York, 1989).
- [36] J.P. Perdew, in *Electronic Structure of Solids '91*, edited by P. Ziesche and H. Eschrig

- (Akademie Verlag, Berlin, 1991), p. 11.
- [37] K. Burke, J.P. Perdew and Y. Wang, in *Electronic Density Functional Theory: Recent Progress and New Directions*, edited by J.F. Dobson, G. Vignale and M.P. Das (Plenum, 1998).
- [38] C. Møller and M.S. Plesset Phys. Rev. **46**, 618 (1934).
- [39] K.P. Huber and G. Herzberg, *Molecular Spectra and Molecular Structure. IV. Constants of Diatomic Molecules*, (Van Nostrand Reinhold, New York, 1979)
- [40] J.L. Martins, J. Buttet and R. Car, Phys. Rev. B **31**, 1804 (1985)
- [41] V. Bonačić-Koutecký, P. Fantucci, J. Koutecký, Phys. Rev. B **37**, 4369 (1988)
- [42] N.W. Ashcroft and N.D. Mermin, *Solid State Physics*, (Saunders College Publishing, New York, 1976)
- [43] C. Kittel, *Introduction to Solid State Physics*, 7th edn., (John Wiley and Sons, New York, 1996)
- [44] S.M. Reimann, M. Koskinen, H. Häkkinen, P.E. Lindelof and M. Manninen, Phys. Rev. B **56**, 12147 (1997).
- [45] J.P. Perdew and A. Zunger, Phys. Rev. B **23**, 5048 (1981).
- [46] D.M. Ceperley and B.J. Alder, Phys. Rev. Lett. **45**, 566 (1980).
- [47] J.P. Perdew Phys. Rev. B **33**, 8822 (1986).
- [48] R. Car and M. Parrinello, Phys. Rev. Lett. **55**, 2471 (1985).
- [49] J.P. Perdew, K. Burke and M. Ernzerhof, Phys. Rev. Lett. **77**, 3865 (1996); *ibid.*, **78**, 1396(E) (1997).